Title
It is not σ8: constraining the non-linear matter power spectrum with the Dark Energy Survey Year-5 supernova sample

Journal
Monthly Notices of the Royal Astronomical Society, 537(4)

ISSN
0035-8711

Authors
Shah, P
Davis, TM
Vincenzi, M
et al.

Publication Date
2025-02-17

DOI
10.1093/mnras/staf286

Monthly Notices of the ROYAL ASTRONOMICAL SOCIETY

MNRAS **537**, 3814–3825 (2025) https://doi.org/10.1093/mnras/staf286
Advance Access publication 2025 February 17

It is not σ_8: constraining the non-linear matter power spectrum with the Dark Energy Survey Year-5 supernova sample

P. Shah ,[1★] T. M. Davis ,[2] M. Vincenzi ,[3] P. Armstrong ,[4] D. Brout ,[3,5] R. Camilleri ,[2] L. Galbany,[6,7] M. S. S. Gill,[8] D. Huterer,[9] N. Jeffrey,[1] O. Lahav,[1] J. Lee,[10] C. Lidman,[4,11] A. Möller,[12] M. Sullivan,[13] L. Whiteway,[1] P. Wiseman,[13] S. Allam,[14] M. Aguena,[15] J. Annis,[14] J. Blazek,[16] D. Brooks,[1] A. Carnero Rosell,[15,17,18] J. Carretero,[19] C. Conselice,[20,21] L. N. da Costa,[15] M. E. S. Pereira,[22] S. Desai,[23] H. T. Diehl,[14] P. Doel,[1] S. Everett,[24] I. Ferrero,[25] B. Flaugher,[14] J. Frieman,[14,26] J. García-Bellido,[27] E. Gaztanaga,[6,7,28] G. Giannini,[19,26] D. Gruen,[29] R. A. Gruendl,[30,31] G. Gutierrez,[14] S. R. Hinton,[2] D. L. Hollowood,[32] K. Honscheid,[33,34] D. J. James,[5] S. Lee,[35] J. L. Marshall,[36] J. Mena-Fernández,[37] R. Miquel,[19,38] A. Palmese,[39] A. Pieres,[15,40] A. A. Plazas Malagón,[8,41] A. Porredon,[42,43] S. Samuroff,[16,19] E. Sanchez,[42] I. Sevilla-Noarbe,[42] M. Smith,[44] E. Suchyta,[45] M. E. C. Swanson,[30] G. Tarle,[9] D. L. Tucker,[14] and N. Weaverdyck[46,47] (DES Collaboration)

Affiliations are listed at the end of the paper

Accepted 2025 February 9. Received 2025 January 30; in original form 2024 November 27

ABSTRACT

The weak gravitational lensing magnification of Type Ia supernovae (SNe Ia) is sensitive to the matter power spectrum on scales $k > 1h$ Mpc^{-1}, making it unwise to interpret SNe Ia lensing in terms of power on linear scales. We compute the probability density function of SNe Ia magnification as a function of standard cosmological parameters, plus an empirical parameter $A_{\rm mod}$ which describes the suppression or enhancement of matter power on non-linear scales compared to a cold dark matter only model. While baryons are expected to enhance power on the scales relevant to SN Ia lensing, other physics such as neutrino masses or non-standard dark matter may suppress power. Using the Dark Energy Survey Year-5 sample, we find $A_{\rm mod} = 0.77^{+0.69}_{-0.40}$ (68 per cent credible interval around the median). Although the median is consistent with unity there are hints of power suppression, with $A_{\rm mod} < 1.09$ at 68 per cent credibility.

Key words: gravitational lensing: weak – galaxies: haloes – cosmology: cosmological parameters – cosmology: dark matter – transients: supernovae.

1 INTRODUCTION

The cosmic microwave background (CMB) together with the expansion history of the Universe at redshifts $z < 2$, as resolved by Type Ia supernovae (SNe Ia) or baryon acoustic oscillations (BAO), suggest the Universe is geometrically flat, and in the main consistent with cold dark matter (CDM) and a cosmological constant Λ as the dominant energy components at late times. While some hints have arisen recently of an evolving dark energy component (Rubin et al. 2023; Camilleri et al. 2024; DES Collaboration 2024; DESI Collaboration 2024) or physics that mimics it, if the Universe is not ΛCDM it is at least very close to it in expansion history.

Nevertheless, measurements of the clustering of matter in ΛCDM differ between those measured in the late Universe and those predicted from the spectrum of $\mathcal{O}(10^{-5})$ CMB temperature and polarization fluctuations projected to the present day using the inferred expansion history and standard gravity (see Abdalla et al. 2022, and references therein). One measure of matter clustering is the dimensionless parameter σ_8, which is the dispersion of the fractional fluctuation of the matter density $\delta = (\rho_{\rm m} - \bar{\rho}_{\rm m})/\bar{\rho}_{\rm m}$ at the present day in spheres of size $8h^{-1}$ Mpc, if structures had grown solely by the *linear* growth rate. Clustering in the late Universe can be measured by weak gravitational lensing, which constrains a combination of this and the present day matter density $\Omega_{\rm m}$ as $S_8 = \sigma_8\sqrt{\Omega_{\rm m}/0.3}$. In particular, a re-analysis of *Planck* satellite data (Efstathiou & Gratton 2021) gives

$$S_8 = 0.828 \pm 0.016 \text{ (Planck TTTEEE)} , \quad (1)$$

whereas for the late Universe the Dark Energy Survey (DES; Abbott et al. 2022) finds

$$S_8 = 0.779^{+0.014}_{-0.015} \text{ (DES Y3 3x2pt)} . \quad (2)$$

These are discrepant by ~ 6 per cent (2.3σ), and the results for other weak lensing surveys (Asgari et al. 2021; Dalal et al. 2023; Li et al. 2023) are consistent with the DES result.

★ E-mail: paul.shah.19@ucl.ac.uk

One possible explanation for the difference is that the systematics of galaxy weak lensing measurements may have been underestimated: although different surveys use different analytical choices, some inherent commonality of pipeline remains between them. However, recent progress on photometric redshift calibration (Hildebrandt et al. 2021; Myles et al. 2021), shear measurements (Mandelbaum et al. 2018; Kannawadi et al. 2019; MacCrann et al. 2022), and intrinsic alignments (for example see Paopiamsap et al. 2024) suggest systematics are not enough to account for the size of the difference, although different pipeline choices may lower the discrepancy to the 1.7σ level (Dark Energy Survey and Kilo-Degree Survey Collaboration 2023).

Another possibility is that the growth of structure on *linear scales* $k < 0.1h$ Mpc^{-1} differs from the ΛCDM expectation, perhaps due to modified gravity. Structure on linear scales in the late Universe is also measured by the four-point correlation function of CMB temperature fluctuations, induced by weak lensing. Results from the *Planck* satellite (Planck Collaboration VIII 2020b), South Pole Telescope (Pan et al. 2023), and the Atacama Cosmology Telescope (ACT; Darwish et al. 2021; Madhavacheril et al. 2024) are all consistent with the *Planck* TTTEEE power spectrum in a ΛCDM background, as stated in equation (1). Although the CMB lensing sensitivity peaks between $1 < z < 3$, this range is sufficiently close to the redshift range of galaxy surveys to disfavour non-ΛCDM linear growth as an explanation.

A remaining possibility is that structure on *non-linear scales* $k > 0.1h$ Mpc^{-1} is different from theoretical expectations. While galaxy weak lensing pipelines discard data at highly non-linear scales (the choice of cut varies from survey to survey), they retain data for some distance into the non-linear regime. While the growth of CDM-only matter fluctuations under standard gravity is well-understood, even down to very small scales (Liu et al. 2024), other physical processes may influence the power spectrum on these scales.

In particular, the presence of baryons modifies the CDM-only expectation. The influence of baryons is qualitatively understood as (1) the suppression of structure on *intermediate scales* $0.1 < k < 10^2h$ Mpc^{-1} by the pressure of 'sub-grid' (meaning below the resolution of the hydrodynamic simulations) energetic outflows from active galactic nucleii and supernovae, and (2) the enhancement of structure on *small scales* $k > 10^2h$ Mpc^{-1} by condensation due to cooling. The strength of these two effects, collectively termed baryon feedback, differs between simulations (see next Section), and the methodology to make quantitative predictions of the changes they induce in the matter power spectrum remains an active subject of research (for example see Eifler et al. 2015; Schneider & Teyssier 2015; Mohammed & Gnedin 2018; Schneider et al. 2019; Aricò et al. 2021; Lu & Haiman 2021; Mead et al. 2021; Lu, Haiman & Zorrilla Matilla 2022).

In this work, we make no assumptions baryonic feedback is necessarily the only physics at work on the small-scale power spectrum. The nature of dark matter itself remains elusive. It may be 'warm' rather than cold, may interact with itself, or may be made of ultralight particles whose de Broglie wavelength is so large that quantum effects influence their clustering properties. These non-standard dark matter models usually suppress power on small-scales. Furthermore, it is well-known that non-zero neutrino mass suppresses small-scale power by reducing CDM-only fluctuations below the scale of their free-streaming length. These effects are difficult to disentangle from baryon feedback at the scales used in current weak lensing surveys (but see Euclid Collaboration 2024, 2025, for future prospects).

Therefore, in this paper, we use a parameter that is physics-agnostic but encapsulates observational differences with the CDM-only non-linear power spectrum. Amon & Efstathiou (2022) have proposed a simple empirical model for the power spectrum as

$$P(k, z) = P_{\rm L}(k, z) + A_{\rm mod}\,[P_{\rm NL}(k, z) - P_{\rm L}(k, z)]\ . \tag{3}$$

Here, $P_{\rm L}$ is that predicted by the spectrum of perturbations of the CMB evolved according to linear theory in a flat ΛCDM background expansion, and $P_{\rm NL}$ is the dark matter only non-linear power spectrum enhanced by collapsed and virialized haloes. $A_{\rm mod,I}$ is a scalar that captures suppression (or enhancement) of structure formation compared to a CDM-only benchmark. It is expressed above as being independent of scale and redshift.

Using data from DES, priors on S_8 and $\Omega_{\rm m}$ from *Planck*, and omitting the scale cuts used in the canonical analysis of DES data (see equation 2), Preston, Amon & Efstathiou (2023) find

$$A_{\rm mod,I} = 0.858 \pm 0.052\,,\ S_8 = 0.811 \pm 0.01\ , \tag{4}$$

where we have used the subscript I to denote this result is derived from intermediate scales.

In isolation, this result represents a repack of the S_8 tension by the introduction of the $A_{\rm mod}$ nuisance parameter: that the value of S_8 is consistent with the CMB is unsurprising given the prior. It was also not possible to say the $A_{\rm mod}$ model was preferred by the data: the χ^2 fit is slightly worse compared to the same data analysed without the *Planck* prior and $A_{\rm mod} = 1$ (see rows 4 and 6 of table 2 of Preston et al. 2023). However, the value of $A_{\rm mod,I}$ seems consistent with the median of a range of hydrodynamical simulations (see fig. 2 of Preston et al. 2023) for the scales the data applies to. Similar conclusions were previously reached with a re-analysis of data from the Kilo Degree Survey (KiDs) by Amon & Efstathiou (2022).

Our motivation in this paper is to examine the $A_{\rm mod}$ model using the weak lensing of SNe Ia. It has been recently detected at $\sim 6\sigma$ significance that SNe Ia are weakly lensed by foreground matter (Shah et al. 2024b). The SNe Ia are dimmer if seen through voids, and brighter if seen on overdense lines of sight (LOS). We will show in the next section that the size of this variation depends on the amplitude of the matter power spectrum on *non-linear scales* rather than the linear scales described by σ_8 or S_8.

Weak lensing generates a non-Gaussian distribution of SN Ia magnitudes that is both generic in shape (that is, not strongly dependent on the modelling choices) and increasing in influence with redshift. As such, it may be distinguished from intrinsic non-Gaussian properties of SNe Ia (which are assumed not to vary with redshift). We forward model the probability density function (pdf) of lensing $p_{\rm lens}(\Delta m)$ conditioned on the primordial power spectrum amplitude A_s, the matter density $\Omega_{\rm m}$ (which is also constrained by the SN Ia Hubble diagram) and $A_{\rm mod}$. This pdf is then convolved with the intrinsic and observational noise of SN Ia data to generate a theoretical distribution of Hubble diagram residuals that may be compared to the data. We will impose priors from the CMB for A_s and $\Omega_{\rm m}$ and marginalize over them, fixing the spectral index $n_s = 0.9665$ (Planck Collaboration VI 2020a) and the sum of neutrino masses $\Sigma m_\nu = 0.06$ eV (we discuss the sensitivity of our results to priors in Appendix A2). Our result is a posterior pdf for $A_{\rm mod}$.

Our paper is organized as follows. In Section 2, we describe the construction of our model. In Section 3, we briefly describe the data, and in Section 4, we present the results of our analysis, and discuss them in Section 5.

By linear scales, we mean $k < 0.1h$ Mpc^{-1}, and we distinguish non-linear scales as intermediate: $0.1 < k < 10^2h$ Mpc^{-1}, and small:

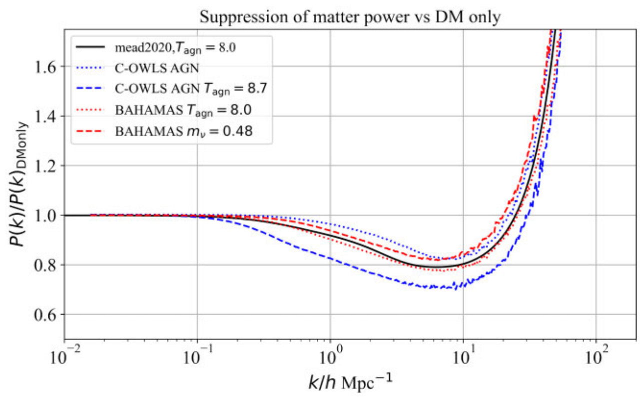

Figure 1. The suppression or enhancement of the power spectrum compared to the dark matter only model of Mead et al. (2020). The models used are HMCODE2020 with $T_{\rm AGN} = 8.0$, the COSMIC-OWLS hydrodynamical simulations (Le Brun et al. 2014), and the BAHAMAS hydrodynamical simulations (McCarthy et al. 2017). Power is suppressed on scales $0.1 < k/h < 30\,{\rm Mpc}^{-1}$ by AGN and supernovae feedback prescriptions, which differ from model to model. At scales $k/h > 30$ Mpc^{-1} power is enhanced due to condensation from baryonic cooling, although again the extent of this depends considerably on the model.

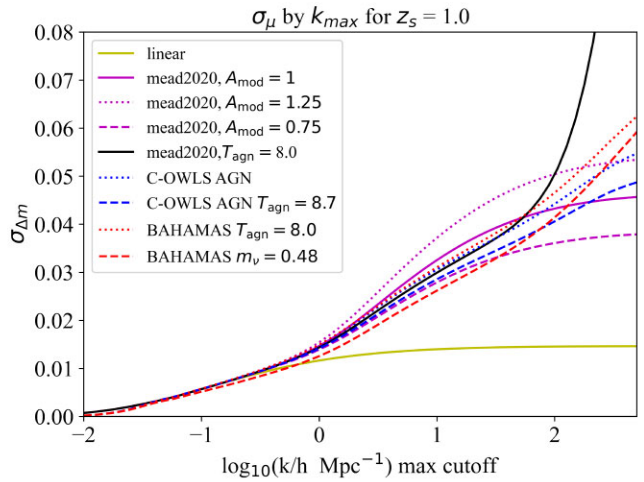

Figure 2. The dispersion of lensing magnification derived from equation (5) as a function of the integral cut-off $k_{\rm max}$ with the lens at $z_l = 0.5$ and the source at $z_s = 1.0$, for a range of models and simulations of the matter power spectrum. The linear power spectrum is shown in yellow, the model of Mead et al. (2020) is shown without baryon feedback in magenta, and with feedback in black dotted and dashed magenta lines show the model adjusted for two choices of $A_{\rm mod}$, as defined in equation (3). Results from power spectra compiled from hydrodynamical simulations and published in van Daalen, McCarthy & Schaye (2020), for a selection of parameters, are shown in red and blue. It is clear that the value of $\sigma_{\Delta m}$ is sensitive to the power spectrum on intermediate and small scales. In particular, while baryonic feedback suppresses lensing on intermediate scales, it enhances it on the small scales relevant to SN Ia. It is not clear that all of the models converge at small scales: in the case of Mead et al. (2020) we have extrapolated the emulator far beyond the region it was designed to model. In the case of simulation data, it is likely that the softening length and particle size produce spurious additional power on small scales. This graph is for illustration only and does not form part of our analysis.

$k > 10^2 h$ Mpc^{-1}. The reduced Hubble constant is $h = H_0/100$ km s^{-1} Mpc^{-1}. We set $c = 1$ everywhere.

2 THEORY

2.1 What does the weak lensing of SNe Ia constrain?

The parameter σ_8 is an integral measure of the amplitude of the linear power spectrum,[1] and therefore directly relatable to the amplitude A_s and shape of the primordial spectrum.

We express the change in magnitude Δm due to lensing of a given SN Ia as relative to a homogeneous universe of the same average matter density. Δm can then be positive (the LOS passes through an overdense region) or negative (through a void). To linear order, averaging over sources we have $\langle \Delta m \rangle = 0$ as gravitational lensing conserves photons. The square of the dispersion $\sigma_{\Delta m}$ of Δm over many sources located at comoving distance χ_s may be written as an integral over the power spectrum (Frieman 1996):

$$\sigma^2_{\Delta m} = 9\pi (0.4 \log 10)^2\, \Omega_{\rm m}^2 H_0^4 \int_0^{\chi_s} {\rm d}\chi \frac{\chi^2(\chi_s - \chi)^2}{\chi_s^2} (1 + z(\chi))^2 \int_0^{k_{\rm max}} {\rm d}k \frac{\Delta^2(k, z)}{k^2}\ , \quad (5)$$

where $\Delta^2(k, z) = k^3 P(k, z)/2\pi^2$ is the dimensionless matter power spectrum, and we have chosen to cut-off the scale at $k_{\rm max}$. The pre-factors of (0.4 log 10) arise as $\sigma_{\Delta m}$ is the dispersion in magnitudes rather than flux amplification. The value of this integral depends considerably on the power spectrum at small scales.

To illustrate this for the case of baryon feedback, we select a range of models from the HMCODE2020[2] emulation package.[3] We choose three options: (1) linear only, (2) the CDM-only non-linear model of Mead et al. (2020), and (3) the baryon feedback model of the same with $T_{\rm AGN} = 8.0$. While HMCODE2020 is not designed to extrapolate to the $k_{\rm max}$ relevant for us, it nevertheless provides a useful illustration of uncertainty on small scales. To this, we add power spectrum data[4] compiled from hydrodynamical simulations by Daalen et al. (2020). The simulations we select are the COSMIC-OWLS suite (Le Brun et al. 2014) and the BAHAMAS suite (McCarthy et al. 2017), which encompass a reasonable range of outcomes. We plot the ratio of the baryon feedback power spectra at $z = 0$ to the relevant CDM-only reference model in Fig. 1. The figure shows power is suppressed up to scales of $k \sim 30h$ Mpc $^{-1}$, then strongly enhanced with considerable difference between models. Equivalent figures for non-standard dark matter models and neutrino masses can be found in Euclid Collaboration (2024, 2025).

In Fig. 2, we plot $\sigma_{\Delta m}$ as a function of the small-scale cut-off $k_{\rm max}$ for the same selection of models. There are considerable differences between models: while the dark matter only model has little sensitivity to scales $k > 10^2 h$ Mpc $^{-1}$, results from baryonic feedback or neutrino prescriptions vary considerably. The apparent

[1]The historical definition of σ_8 as the dispersion of density fluctuations in spheres of $8h^{-1}$ Mpc – as proxied by galaxy counts – was motivated by the earliest galaxy surveys. It was soon understood that this was difficult to express theoretically: fluctuations on this scale are enhanced by non-linear gravitational evolution and differ by the type of galaxy being counted due to galaxy bias. By re-defining σ_8 in terms of the *linear* power spectrum, the modern definition effectively refers to structure on scales larger than $8h^{-1}$ Mpc.

[2]https://github.com/alexander-mead/HMcode

[3]As implemented in CAMB, https://github.com/cmbant/CAMB.

[4]https://powerlib.strw.leidenuniv.nl

runaway behaviour of the model of Mead et al. (2020) is due to a flattening of the power spectrum at $k > 10^2 h$ Mpc $^{-1}$ because the stellar component is represented as a delta function (the authors make no claims their model can be extrapolated beyond $k\ sim 20$). The simulation results start to diverge at $k > 250h$ Mpc $^{-1}$. This is likely due to the softening lengths ($r = 4$ kpc for COSMIC-OWLS and BAHAMAS) and particle masses ($4\times10^9 - 7\times10^8 \mathrm{M}_\odot$) used in them which lead to spurious clumping on small scales. We estimate that to obtain adequate predictions of SN Ia lensing from *N*-body or hydrodynamical simulations would require particle masses of $m_p \sim 10^7 \mathrm{M}_\odot$ and softening lengths of 1 kpc (corresponding to $k \sim 10^3 h$ Mpc^{-1}). This applies either to estimation from the power spectrum or directly through ray-tracing. We conclude that a reliable a priori calculation of $\sigma_{\Delta m}$ is at present unavailable, and we emphasize that we do not make use of any of these models or equation (5) in our analysis.

It is also clear from Fig. 2 that SN Ia weak lensing is insensitive to the linear regime and associated cosmological parameters such as σ_8. Indeed, linear-scale correlation is undetectable with current data sets (Shah et al. 2024b). In this paper, we will fix the linear scales using a prior on A_s from the CMB, and use SNe Ia to constrain the non-linear empirical amplitude $A_{\rm mod}$.

Before continuing, we note that the existence of compact objects (CO, for example primordial black holes, if they exist) produces an enhancement in $\sigma_{\Delta m}$ if they form a significant fraction $\alpha = \Omega_{\rm CO}/\Omega_{\rm m}$ of the matter density. In Shah et al. (2024a), it was shown that $\alpha < 0.12$ at 95 per cent credibility, and $\alpha = 0$ was preferred (by the Bayes ratio of model probabilities) to $\alpha > 0$. Hence, while some compact objects (e.g. stars) certainly exist, they do not make a measurable contribution to SN Ia lensing. We therefore neglect them in this analysis.

2.2 SN Ia weak lensing as a function of $A_{\rm mod}$

In the halo model description, matter power is the sum of linear low density-contrast perturbations, plus gravitationally bound high density-contrast haloes that have collapsed and virialized (Kaiser 1984). This is also taken as the starting point for the codes used in weak lensing shear analyses such as HMCODE2020, which adjusts the theoretical halo-model power spectrum empirically to better fit simulations (Mead et al. 2020). We write our power spectrum model as denoted by subscripts L and H respectively:

$$P(k, z) = P_{\rm L}(k, z) + A_{\rm mod} P_{\rm H}(k, z)\ . \tag{6}$$

$P_{\rm L}$ is the same as that in equation (3), while $P_{\rm H}$ is the contribution solely due to haloes, and equivalent to the term $P_{\rm NL} - P_{\rm L}$ in equation (3). For $P_{\rm H}$ we adopt the calibration of Sheth, Mo & Tormen (2001) refitted by Courtin et al. (2011), which describes the abundance and spectrum of haloes in a purely CDM universe very well over a huge range of halo masses (Zheng et al. 2024). The calibration of Sheth et al. (2001) was also used as the starting point for power spectrum emulator models such as Smith et al. (2003) and successors. We take the haloes to have the Navarro-Frenk-White (NFW) profile described in Navarro, Frenk & White (1997), as it was shown in Shah et al. (2024b) that the NFW model is consistent with observations of SN Ia lensing. Although in general the profiles will not be spherically symmetric, this is an accurate approximation after averaging over many LOS (Mandelbaum et al. 2005).

Our aim is to model the statistics of magnitude fluctuations of SNe Ia in terms of $A_{\rm mod}$. Before we proceed to the details below, we note that whilst our $A_{\rm mod}$ is equivalent in formulation to that of Amon & Efstathiou (2022), important practical differences arise when applied to SNe Ia data. The integral of equation (5) does not define a window function of scale other than limits imposed by the size of the source and lens, and other statistics of SN Ia lensing operate in the same fashion. This is distinct from the scales introduced by spatial correlations functions of transverse separation used in galaxy surveys, which may then be used to set scale cuts. Fig. 2 indicates that for intermediate scales, there is a broad expectation that baryonic feedback will result in $A_{\rm mod} < 1$ (the models considered generate less lensing than the CDM-only model of Mead et al. 2020). Conversely, continuing to small scales relevant for SN Ia lensing, it is likely that baryons alone would lead to $A_{\rm mod} > 1$ (more lensing is observed than expected in a CDM-only universe), although we noted above that the resolution limits of the simulations may generate spurious power enhancement on these scales. Alternatively, warm dark matter (if it exists) and neutrino masses are expected to suppress power on small scales, reducing $A_{\rm mod}$. We therefore have no a priori expectations of whether the $A_{\rm mod,S}$ we measure from SNe Ia will indicate power suppression or enhancement.

Following the procedure of Zumalacárregui & Seljak (2018), revised in Shah et al. (2024a), we model the full-shape of the lensing pdf[5] as a function of cosmological parameters, intrinsic skew and $A_{\rm mod}$. We write the lensing pdf as a convolution of lensing due to linear scales and haloes as

$$p_{\rm lens}(\Delta m) = p_{\rm L}(\Delta m; A_s, \Omega_{\rm m}, z) * p_{\rm H}(\Delta m; A_s, \Omega_{\rm m}, A_{\rm mod}, z)\ , \tag{7}$$

where $*$ denotes the convolution operation. The one-point distribution of weak lensing convergence on linear scales has been shown to be well-approximated by a log-normal distribution (Clerkin et al. 2017). We therefore take $p_{\rm L}$ as a log-normal distribution of zero mean and dispersion $\sigma_{\rm L}$ obtained from equation (5) using the linear power spectrum. We obtain $p_{\rm H}$ from TURBOGL[6] (Kainulainen & Marra 2009, 2011) which uses semi-analytic integration to accurately model lensing by dark matter haloes (and thus avoids the resolution issues inherent in *N*-body or hydrodynamical simulations). The minimum halo mass has been set to be $10^7 \mathrm{M}_\odot$. $A_{\rm mod}$ is then a simple scale parameter on this pdf such that $\sigma_{\rm H}(A_{\rm mod}) = A_{\rm mod}\sigma_{\rm H}(A_{\rm mod} = 1)$.

Intrinsic skew of SN Ia residuals may in principle be confused with lensing. However, while lensing skew is redshift-dependent, intrinsic skew is presumed not to be. We parametrize the intrinsic dispersion of SN Ia by the sin-arcsin distribution family (Jones & Pewsey 2009) where δ, ϵ of this family capture both skew and kurtosis with $\delta = 1, \epsilon = 0$ being a normal distribution. The distribution is defined as

$$p_{\rm Int}(\Delta m) = \frac{1}{\sqrt{2\pi}E}\delta\sqrt{1+x^2}\exp(-x^2/2)/\sqrt{1+\Delta m^2}\ , \tag{8}$$

where

$$x = (\sinh(\delta \mathrm{arcsinh}(\Delta m) - \epsilon) - D)/E\ , \tag{9}$$

and the location and scale parameters D, E are determined by the constraints

$$\begin{aligned} &\int \Delta m\, p_{\rm Int}(\Delta m) d\Delta m = 0 \\ &\int \Delta m^2 p_{\rm Int}(\Delta m) d\Delta m = \sigma_i^2\ . \end{aligned} \tag{10}$$

Here, $\sigma_i^2 = C_{ii}$ is the diagonal of the SN Ia covariance matrix (see Section 2.3 below), which is the statistical uncertainty in the SN Ia

[5] We avoid using methods based on higher order moments of the pdf (such as described in Marra, Quartin & Amendola 2013; Quartin, Marra & Amendola 2014), which are vulnerable to the presence of outliers.
[6] https://github.com/valerio-marra/turboGL

distance modulus. Convolving this with the lensing pdf gives

$$p_{\rm res}(\Delta m) = p_{\rm lens} * p_{\rm Int} \ , \tag{11}$$

with Δm now the Hubble diagram residual

$$\Delta m = m_i - \mathcal{M} - \mu_{i,\rm theory}(\theta) \ . \tag{12}$$

Here, $\mathcal{M} = M - 5\log_{10} H_0$ is a degenerate combination of the Hubble constant H_0 and the fiducial SN Ia absolute magnitude M. The distance modulus is $\mu_{i,\rm theory} = 5\log_{10}(D_{\rm L}(z_i, \Omega_{\rm M})H_0/c) + 25$ and we take $D_{\rm L}$ as the usual homogeneous cosmology luminosity distance in a flat ΛCDM model.

2.3 The SN Ia likelihood adjusted for lensing

Denoting the model parameters collectively as θ, the SN Ia likelihood for a homogeneous cosmology using the DES SN Ia Year-5 sample (DES-SN5YR) is assigned to be the Gaussian

$$\ln \mathcal{L}_G(\Delta m|\theta) = -\frac{1}{2}\sum_{i,j} \Delta m_i C^{-1}_{ij} \Delta m_j \tag{13}$$

where C is the covariance matrix which is the sum of systematic and statistical errors (Vincenzi et al. 2024). In the presence of non-Gaussian lensing, we adjust this to

$$\log \mathcal{L} = \ln \mathcal{L}_G + \left(\sum_i \log p_{\rm res} - \sum_i \log p_{\rm diag}\right) \ , \tag{14}$$

with

$$p_{\rm diag}(\Delta m_i) = \frac{1}{\sqrt{2\pi}\sigma_i} \exp(-\frac{1}{2}(\Delta m_i/\sigma_i)^2) \ , \tag{15}$$

where $\sigma_i^2 = C_{ii}$ as per equation (10) and $p_{\rm res}$ is defined in equation (11). The term in brackets of equation (14) adjusts the likelihood of each individual SN Ia for the difference between a skewed (either by lensing or intrinsic skew) residual probability and a Gaussian probability. The first term retains covariance, which is important for correct error estimation. As explained in Shah et al. (2024a), this likelihood reduces correctly when there is no lensing or intrinsic skew as in this case $p_{\rm res} = p_{\rm diag}$, and also when the covariance matrix is diagonal as in this case $\log \mathcal{L}_G = \sum_i \log p_{\rm diag}$. The key point is C is only weakly non-diagonal, so we expect our assignment to be accurate. We discuss the validation of this likelihood in Appendix A1.

We pre-compute the lensing pdfs for a grid of redshifts, cosmological parameters and $A_{\rm mod}$, and interpolate the log probabilities. The evaluation of the likelihood takes ~ 0.3 s for $\sim 1,500$ SN Ia on a typical laptop. We fix the optical depth of reionization as $\tau = 0.0561$ and the power spectrum slope as $n_s = 0.9665$, and set the neutrino mass $m_\nu = 0.06$ eV. We take uniform priors as $A_{\rm mod} \in (0.2, 2.5)$ (motivated by consideration of Fig. 2), $\epsilon \in (-0.2, 0.2)$ and $\delta \in (0.6, 1.4)$. Runs are performed using POLYCHORD[7] (Handley, Hobson & Lasenby 2015), and plots and analysis are made using ANESTHETIC[8] (Handley 2019).

3 DATA

3.1 SN Ia

We use the DES-SN5YR data set as described in Sánchez et al. (2024), but with the modification not to exclude SNe Ia that are more than 4σ away from the best-fit Hubble diagram. Removing this cut avoids biasing our results by arbitrarily truncating the skewed and extended distribution of residuals that lensing produces. The SN Ia survey was conducted in four regions of the DES footprint with a total of 10 fields, and the SN Ia range from $0.01 < z < 1.13$. Supernova candidates are analysed using machine-learning classifiers (Möller & de Boissière 2020; Qu et al. 2021; Möller et al. 2022) whose inputs are the light curve observations, and whose output is the probability of being an SN Ia. The diagonal of the covariance is then adjusted for this probability, down-weighting likely contaminants but not discarding them altogether. The SN Ia redshift is set to be the spectroscopic redshift of the galaxy that is closest in directional light radius to the SN Ia (Sullivan et al. 2006; Qu et al. 2024).

There are 1930 SN in the initial sample, of a similar redshift distribution to the original DES-SN5YR data set, and we cut these to include only those between $0.2 < z < 1.0$ in our analysis. The lower cut is because lensing will not materially affect low redshift SN Ia, and the lower redshift SN Ia are from older, heterogeneous surveys with uncertain selection functions. The upper cut is to reduce potential uncertainties due to larger bias corrections at high redshifts (for example see fig. 7 of Vincenzi et al. 2024). We additionally cut likely contaminants or poorly measured SN Ia, by excluding data with $\sigma_m > 1.0$ mag and $p(\text{SN Ia}) < 0.9$. Our data input to the lensing likelihood therefore comprises 1484 SN Ia of average redshift $z \sim 0.47$.

3.2 CMB

As input priors to H_0, $\Omega_{\rm m}$ and linear scales A_s, we use chains derived from the PYTHON implementation of Planck's 2015 `Plik_lite` (Prince & Dunkley 2019) which may be found on the repository of the DES-SN5YR data.[9] These chains have somewhat wider constraints than the fiducial results of Planck Collaboration VI (2020a), but are perfectly adequate for our results.

4 RESULTS

Marginalizing over all other parameters, and quoting the median, 16 per cent and 84 per cent quantiles, we find

$$A_{\rm mod,S} = 0.77^{+0.69}_{-0.40} \tag{16}$$

which is consistent within 1σ of the CDM-only value of $A_{\rm mod} = 1$, and we have used the subscript S to denote our result is derived primarily from small scales. We show the triangle plot for the marginalized posterior and pair distributions in Fig. 3.

There are hints the data prefers lower values with the maximum of the full posterior (as determined by a kernel density estimate) at $A_{\rm mod,S} = 0.30$, and the highest-density 68 per cent credible interval is $A_{\rm mod,S} < 1.09$. We expect this upper bound to be conservative, as Fig. 3 shows our posterior is truncated by our prior and it is likely that more probability mass might be found below our prior range rather than above it. Conversely, our credible interval around the median will be somewhat overoptimistic for the same reason.

Notably, our method demonstrates that SN Ia can distinguish the effects of the linear and non-linear parts of the power spectrum, as S_8 and $A_{\rm mod,S}$ show little correlation in their posteriors. The credible intervals for the intrinsic skew parameters $\epsilon = -0.07^{+0.04}_{-0.04}$ and $\delta = 0.91^{+0.06}_{-0.05}$ are moderately discrepant from the values (0,1) of

[7] https://github.com/PolyChord/PolyChordLite
[8] https://github.com/handley-lab/anesthetic
[9] https://github.com/des-science/DES-SN5YR

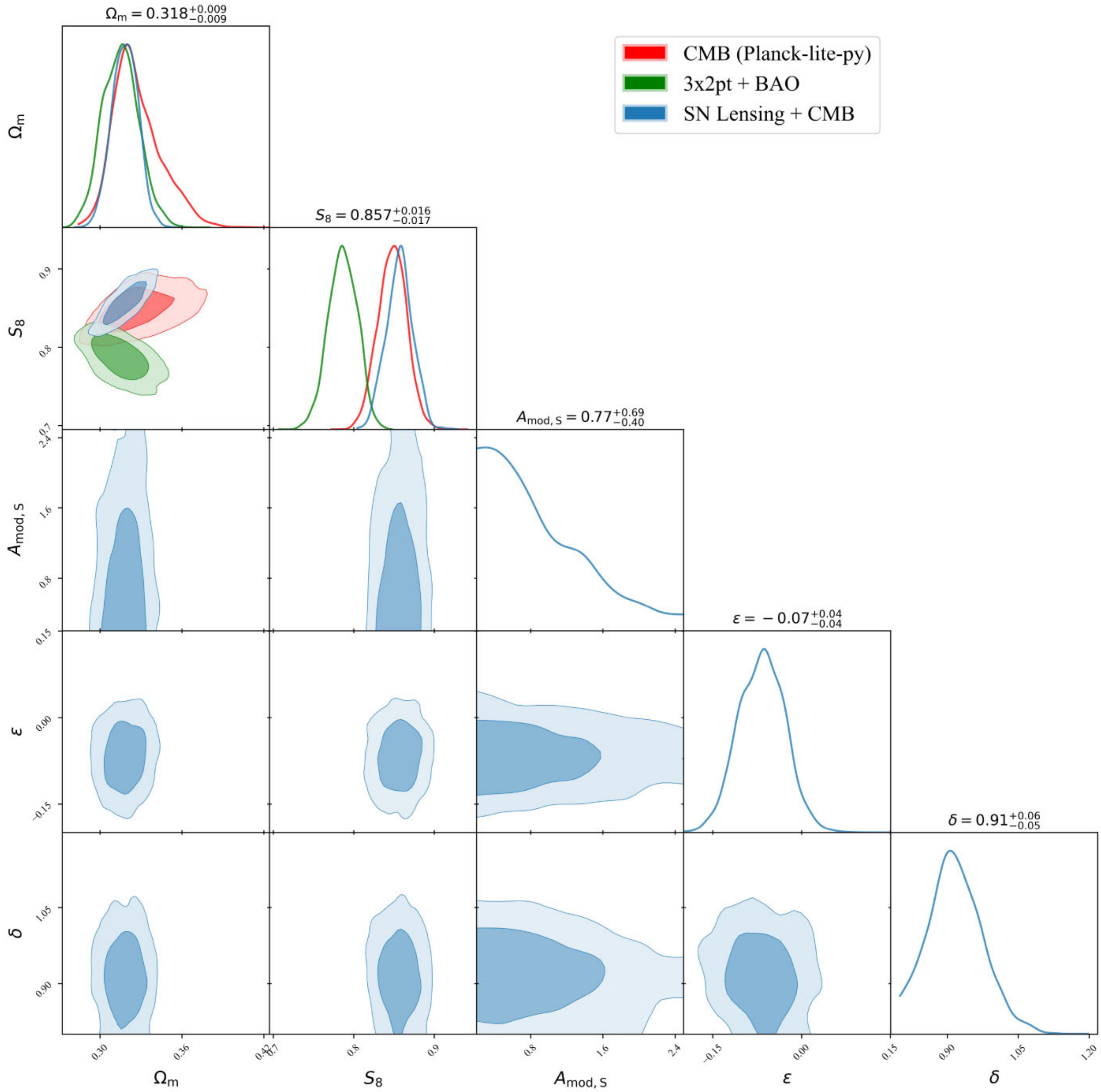

Figure 3. A triangle plot of the posteriors for relevant model parameters, with the medians and 68 per cent quantiles shown along the diagonal. The constraints on S_8 and Ω_m arise from the fit of the CMB power spectrum and SN Ia luminosity distances. The CMB priors we use are shown in red. As noted in the text, the *Planck*-lite-py likelihood used to generate the chains has moderately wider constraints than the full likelihood used in Planck Collaboration VI (2020a), however this does not impact our results. In contrast, the constraint on $A_{mod,S}$ arises from the detail of the distribution of SN Ia residuals around the mean and is not degenerate with S_8. ϵ and δ represent intrinsic skew and kurtosis of the distribution; it is evident from the posterior that there is little degeneracy between this and lensing. For comparison, we also plot a combination (in green) of the DES 3×2pt analysis of Abbott et al. (2022) and BAO measurements from the Sloan Digital Sky Survey (SDSS), as summarized in Alam et al. (2021). We remind the reader that we have defined $A_{mod} = 1$ as small-scale power that is compatible with the growth of CDM-only fluctuations in a flat ΛCDM universe with cosmological parameters derived from the CMB.

a Gaussian distribution, but at no great significance. There is little covariance between intrinsic skew and matter-power parameters.

Our maximum-likelihood improves the fit over the Gaussian likelihood by $\delta\chi^2 = -5.6$. Subtracting out the fit improvement due to the introduction of intrinsic skew, we find $A_{mod,S} = 0.3$ improves the fit by $\delta\chi^2 = -1.2$ compared to $A_{mod,S} = 1$.

We describe our estimation of systematics in Appendix A, with the dominant contribution being the assignment of the likelihood. While there is some inaccuracy in our posterior, examining the expected coverage probability we see that the 68 per cent highest-density credible interval we quote above is likely to be conservative (over and above the effect of truncation by the prior noted above) by

$\delta A_{\rm mod,S} \sim 0.19$. Other credible intervals of interest have systematics of a similar amount or smaller. We have tested the effect of the redshift and SN Ia probability cuts used for our data and find they are small. Our total systematic error estimate is $\delta A_{\rm mod,S} \sim 0.2$. Therefore, we judge that systematics are smaller than our statistical error by a factor of at least 2.

The literature has to date quoted results in terms of σ_8 which (ignoring for now the caveats we noted in Section 2) this be interpreted as $\sim A_{\rm mod,S}\sigma_{8,\rm CMB}$. The first measurement was done by Castro & Quartin (2014), who found $\sigma_8 = 0.84^{+0.28}_{-0.65}$ using 706 SN Ia from the Joint Lightcurve (JLA) catalogue (Betoule et al. 2014). Re-analysing the JLA data using a model that also incorporated SN Ia peculiar velocities (via their redshifts), Macaulay et al. (2017) found similar results but also that the systematics in Castro & Quartin (2014) were underestimated. In Macaulay et al. (2020), 196 SN Ia from the DES Year 3 release were used in the same methodology to find $\sigma_8 = 1.2^{+0.9}_{-0.8}$. Calibrating a halo model using the observed correlation between SN Ia residuals and foreground galaxy positions, Shah et al. (2024b) found $\sigma_8 = 0.9 \pm 0.13$ by comparing the dispersion $\sigma_{\Delta m}$ of lensing in this model along random lines of sight to a fitting formula given in Marra et al. (2013). In general, although these results do not marginalize over cosmological parameters and intrinsic skew as we have done, they all indicate a weak preference for $A_{\rm mod,S} > 1$. However, they are consistent with our results within 1σ.

5 CONCLUSIONS

In this paper, we have shown that the non-Gaussian distribution of residuals of SNe Ia to the Hubble diagram induced by weak gravitational lensing carries statistical information about the matter power spectrum on scales $k > 1h$ Mpc^{-1}. In particular, SNe Ia data provide access to scales that cannot be probed by galaxy-sized sources. Due to the theoretical uncertainties of modelling the power spectrum on these scales, we have constrained an empirical parameter $A_{\rm mod,S}$, which describes the suppression (or enhancement) of matter power on small scales compared to a benchmark of a dark matter only ΛCDM universe with cosmological parameters derived from the CMB. We find hints of suppression with $A_{\rm mod,S} = 0.77^{+0.69}_{-0.40}$ (median and 68 per cent credible interval), with the posterior peaking at low values of $A_{\rm mod,S}$.

While our results are weaker than those of Preston et al. (2023) (quoted as equation 4 here), who find almost 3σ preference for $A_{\rm mod} < 1$, they are independent of data and the typical systematics of galaxy shear surveys such as photometric redshifts, shape blending, and intrinsic alignments. By contrast, our systematics arise primarily from assignment of the likelihood.

Our results are not precise enough to distinguish between competing models of dark matter or baryonic physics. The pathway to doing so lies in improvements to statistical error, systematics, and theoretical modelling. Regarding statistical error, in Quartin et al. (2014), it was forecast that a sample of 3000 SN Ia from DES would be able to constrain σ_8 to within ~ 35 per cent; this is consistent with our ~ 55 per cent constraint for $A_{\rm mod}$ using 1484 SN Ia. The authors also forecast that a sample of 500 000 SN Ia from the Rubin LSST survey would result in a constraint of ~ 3 per cent. In this case, the statistical error would be below the systematics, and the current likelihood assignment would need to be improved. One way this could be achieved is the use of simulation-based inference.

Finally, regarding theoretical modelling it would be desirable to interpret our results in the context of parameters of physical processes, which requires extending these models to small scales. As noted in Section 2, the apparent non-convergence of the baryonic models illustrated in Fig. 2 is likely due to an extrapolation of emulators beyond the scales they were trained on, because of the resolution limits of hydrodynamical simulations. This is in principle surmountable: promising work has been done on 'nesting' dark matter only simulations to increase resolution (Wang et al. 2020; Zheng et al. 2024) arbitrarily, and it seems plausible that this methodology could be applied to other simulations. Even if this were not possible, we note that certain ranges of $A_{\rm mod}$ would provide severe constraints on the underlying physics: for example $A_{\rm mod} \lesssim 0.5$ is not expected from any of the models considered here with cold dark matter as the dominant component.

We conclude that for future data sets, SN Ia offer a unique window into the power spectrum on small scales, and the pathway to improve the control of systematics and theoretical modelling is clear.

ACKNOWLEDGEMENTS

PS devised the project, performed the analysis, and drafted the manuscript; MV re-analysed the DES-SN5YR data with cuts removed; TMD, RC, DH, LG, NJ, JL, CL, MSu, LW advised on the analysis and commented on the manuscript; PA assisted with the Pippin pipeline used for the simulations. TMD and MSu were also internal reviewers and RM was the final reader. The remaining authors have made contributions to this paper that include, but are not limited to, the construction of DECam and other aspects of collecting the data; data processing and calibration; developing broadly used methods, codes, and simulations; running the pipelines and validation tests; and promoting the science analysis.

This paper has gone through internal review by the DES collaboration, and we thank the anonymous referee for his helpful comments.

We acknowledge the following former collaborators, who have contributed directly to this work – Ricard Casas, Pete Challis, Michael Childress, Ricardo Covarrubias, Chris D'Andrea, Alex Filippenko, David Finley, John Fisher, Francisco Förster, Daniel Goldstein, Santiago González-Gaitán, Ravi Gupta, Mario Hamuy, Steve Kuhlmann, James Lasker, Marisa March, John Marriner, Eric Morganson, Jennifer Mosher, Elizabeth Swann, Rollin Thomas, and Rachel Wolf.

TMD, AC, RC, acknowledge the support of an Australian Research Council Australian Laureate Fellowship (FL180100168) funded by the Australian Government, and AM was supported by the ARC Discovery Early Career Researcher Award (DECRA) project number DE230100055. MS and JL are supported by DOE grant DE-FOA-0002424 and NSF grant AST-2108094. RK was supported by DOE grant DE-SC0009924. MV was partly supported by NASA through the NASA Hubble Fellowship grant HST-HF2-51546.001-A awarded by the Space Telescope Science Institute, which is operated by the Association of Universities for Research in Astronomy, Incorporated, under NASA contract NAS5-26555. LG acknowledges financial support from AGAUR, CSIC, MCIN, and AEI 10.13039/501100011033 under projects PID2023-151307NB-I00, PIE 20215AT016, CEX2020-001058-M, and 2021-SGR-01270. DS was supported in part by NASA grant 14-WPS14-0048. The UCSC team was supported in part by NASA grants NNG16PJ34G and NNG17PX03C issued through the Roman Science Investigation Teams Program; NSF grants AST-1518052 and AST-1815935; NASA through grant No. AR-14296 from the Space Telescope Science Institute, which is operated by AURA, Inc., under NASA contract NAS 5–26555; the Gordon and Betty Moore Foundation; the Heising-Simons Foundation. We acknowledge the University of Chicago's Research Computing Center for their support of this work.

Funding for the DES Projects has been provided by the U.S. Department of Energy, the U.S. National Science Foundation, the Ministry of Science and Education of Spain, the Science and Technology Facilities Council of the United Kingdom, the Higher Education Funding Council for England, the National Center for Supercomputing Applications at the University of Illinois at Urbana-Champaign, the Kavli Institute of Cosmological Physics at the University of Chicago, the Center for Cosmology and Astro-Particle Physics at the Ohio State University, the Mitchell Institute for Fundamental Physics and Astronomy at Texas A&M University, Financiadora de Estudos e Projetos, Fundação Carlos Chagas Filho de Amparo à Pesquisa do Estado do Rio de Janeiro, Conselho Nacional de Desenvolvimento Científico e Tecnológico and the Ministério da Ciência, Tecnologia e Inovação, the Deutsche Forschungsgemeinschaft and the Collaborating Institutions in the Dark Energy Survey.

The Collaborating Institutions are Argonne National Laboratory, the University of California at Santa Cruz, the University of Cambridge, Centro de Investigaciones Energéticas, Medioambientales y Tecnológicas-Madrid, the University of Chicago, University College London, the DES-Brazil Consortium, the University of Edinburgh, the Eidgenössische Technische Hochschule (ETH) Zürich, Fermi National Accelerator Laboratory, the University of Illinois at Urbana-Champaign, the Institut de Ciències de l'Espai (IEEC/CSIC), the Institut de Física d'Altes Energies, Lawrence Berkeley National Laboratory, the Ludwig-Maximilians Universität München and the associated Excellence Cluster Universe, the University of Michigan, NSF's NOIRLab, the University of Nottingham, The Ohio State University, the University of Pennsylvania, the University of Portsmouth, SLAC National Accelerator Laboratory, Stanford University, the University of Sussex, Texas A&M University, and the OzDES Membership Consortium.

Based in part on observations at Cerro Tololo Inter-American Observatory at NSF's NOIRLab (NOIRLab Prop. ID 2012B-0001; PI: J. Frieman), which is managed by the Association of Universities for Research in Astronomy (AURA) under a cooperative agreement with the National Science Foundation. Based in part on data acquired at the Anglo-Australian Telescope. We acknowledge the traditional custodians of the land on which the AAT stands, the Gamilaraay people, and pay our respects to elders past and present. Parts of this research were supported by the Australian Research Council, through project numbers CE110001020, FL180100168, and DE230100055. Based in part on observations obtained at the international Gemini Observatory, a programme of NSF's NOIRLab, which is managed by the Association of Universities for Research in Astronomy (AURA) under a cooperative agreement with the National Science Foundation on behalf of the Gemini Observatory partnership: the National Science Foundation (United States), National Research Council (Canada), Agencia Nacional de Investigación y Desarrollo (Chile), Ministerio de Ciencia, Tecnología e Innovación (Argentina), Ministério da Ciência, Tecnologia, Inovações e Comunicações (Brazil), and Korea Astronomy and Space Science Institute (Republic of Korea). This includes data from programmes (GN-2015B-Q-10, GN-2016B-LP-10, GN-2017B-LP-10, GS-2013B-Q-45, GS-2015B-Q-7, GS-2016B-LP-10, GS-2016B-Q-41, and GS-2017B-LP-10; PI Foley). Some of the data presented herein were obtained at Keck Observatory, which is a private 501(c)3 non-profit organization operated as a scientific partnership among the California Institute of Technology, the University of California, and the National Aeronautics and Space Administration (PIs Foley, Kirshner, and Nugent). The Observatory was made possible by the generous financial support of the W. M. Keck Foundation. This paper includes results based on data gathered with the 6.5 meter Magellan Telescopes located at Las Campanas Observatory, Chile (PI Foley), and the Southern African Large Telescope (SALT) (PIs M. Smith & E. Kasai). The authors wish to recognize and acknowledge the very significant cultural role and reverence that the summit of Maunakea has always had within the Native Hawaiian community. We are most fortunate to have the opportunity to conduct observations from this mountain.

The DES data management system was supported by the National Science Foundation under Grant Numbers AST-1138766 and AST-1536171. The DES participants from Spanish institutions are partially supported by MICINN under grants ESP2017-89838, PGC2018-094773, PGC2018-102021, SEV-2016-0588, SEV-2016-0597, and MDM-2015-0509, some of which include ERDF funds from the European Union. IFAE is partially funded by the CERCA programme of the Generalitat de Catalunya. Research leading to these results has received funding from the European Research Council under the European Union's Seventh Framework Program (FP7/2007-2013) including ERC grant agreements 240672, 291329, and 306478. We acknowledge support from the Brazilian Instituto Nacional de Ciência e Tecnologia (INCT) do e-Universo (CNPq grant 465376/2014-2).

This research used resources of the National Energy Research Scientific Computing Center (NERSC), a U.S. Department of Energy Office of Science User Facility located at Lawrence Berkeley National Laboratory, operated under Contract No. DE-AC02-05CH11231 using NERSC award HEP-ERCAP0023923. This manuscript has been authored by Fermi Research Alliance, LLC under Contract No. DE-AC02-07CH11359 with the U.S. Department of Energy, Office of Science, Office of High Energy Physics.

Facilities: CTIO:4m, AAT, Gemini:Gillett (GMOS-N), Gemini:South (GMOS-S), Keck:I (LRIS), Keck:II (DEIMOS), Magellan:Baade (IMACS), Magellan:Clay (LDSS3, MagE), SALT.

Software: NUMPY (Harris et al. 2020), CAMB (Lewis & Bridle 2002), MATPLOTLIB (Hunter 2007), SCIPY (Virtanen et al. 2020), SNANA (Kessler et al. 2009), PIPPIN (Hinton & Brout 2020), POLYCHORD (Handley et al. 2015), ANESTHETIC (Handley 2019), PLIKLITEPYTHON implementation (Prince & Dunkley 2019), HMCODE2020 (Mead et al. 2020), TURBOGL (Kainulainen & Marra 2009).

DATA AVAILABILITY

The data and PYTHON code used to generate the results and plots in this paper are available on reasonable request from the authors. The lensing pdfs used will be made available upon publication at https://github.com/paulshah/SNLensing.

REFERENCES

Abbott T. M. C. et al., 2022, Phys. Rev. D, 105, 023520
Abdalla E. et al., 2022, J. High Energy Astrophys., 34, 49
Alam S. et al., 2021, Phys. Rev. D, 103, 083533
Amon A., Efstathiou G., 2022, MNRAS, 516, 5355
Aricò G., Angulo R. E., Contreras S., Ondaro-Mallea L., Pellejero-Ibañez M., Zennaro M., 2021, MNRAS, 506, 4070
Asgari M. et al., 2021, A&A, 645, A104
Betoule M. et al., 2014, A&A, 568, A22
Camilleri R. et al., 2024, MNRAS, 533, 2615
Castro T., Quartin M., 2014, MNRAS, 443, L6
Clerkin L. et al., 2017, MNRAS, 466, 1444
Courtin J., Rasera Y., Alimi J. M., Corasaniti P. S., Boucher V., Füzfa A., 2011, MNRAS, 410, 1911
DES Collaboration, 2024, ApJ, 973, L14
DESI Collaboration, 2024, J. Cosmol. Astropart. Phys., 2025, 021

Dalal R. et al., 2023, Phys. Rev. D, 108, 123519
Dark Energy Survey and Kilo-Degree Survey Collaboration, 2023, Open J. Astrophys., 6, 36
Darwish O. et al., 2021, MNRAS, 500, 2250
Efstathiou G., Gratton S., 2021, Open J. Astrophys., 4, 8
Eifler T., Krause E., Dodelson S., Zentner A. R., Hearin A. P., Gnedin N. Y., 2015, MNRAS, 454, 2451
Euclid Collaboration, 2024, preprint (arXiv:2406.18274)
Euclid Collaboration, 2025, A&A, 693, A58
Frieman J. A., 1996, Comments on Astrophysics, 18, 323
García-García C., Zennaro M., Aricò G., Alonso D., Angulo R. E., 2024, J. Cosmol. Astropart. Phys., 2024, 024
Handley W., 2019, J. Open Source Softw., 4, 1414
Handley W. J., Hobson M. P., Lasenby A. N., 2015, MNRAS, 453, 4384
Harris C. R. et al., 2020, Nature, 585, 357
Hildebrandt H. et al., 2021, A&A, 647, A124
Hinton S., Brout D., 2020, J. Open Source Softw., 5, 2122
Hunter J. D., 2007, Comput. Sci. Eng., 9, 90
Jones M. C., Pewsey A., 2009, Biometrika, 96, 761
Kainulainen K., Marra V., 2009, Phys. Rev. D, 80, 123020
Kainulainen K., Marra V., 2011, Phys. Rev. D, 84, 063004
Kaiser N., 1984, ApJ, 284, L9
Kannawadi A. et al., 2019, A&A, 624, A92
Kessler R. et al., 2009, PASP, 121, 1028
Le Brun A. M. C., McCarthy I. G., Schaye J., Ponman T. J., 2014, MNRAS, 441, 1270
Lemos P., Cranmer M., Abidi M., Hahn C., Eickenberg M., Massara E., Yallup D., Ho S., 2023, Machine Learning: Science and Technology, 4, 01LT01
Lewis A., Bridle S., 2002, Phys. Rev. D, 66, 103511
Li X. et al., 2023, Phys. Rev. D, 108, 123518
Liu Y. et al., 2024, MNRAS, 527, 11740
Lu T., Haiman Z., 2021, MNRAS, 506, 3406
Lu T., Haiman Z., Zorrilla Matilla J. M., 2022, MNRAS, 511, 1518
MacCrann N. et al., 2022, MNRAS, 509, 3371
Macaulay E., Davis T. M., Scovacricchi D., Bacon D., Collett T., Nichol R. C., 2017, MNRAS, 467, 259
Macaulay E. et al., 2020, MNRAS, 496, 4051
Madhavacheril M. S. et al., 2024, ApJ, 962, 113
Mandelbaum R., Tasitsiomi A., Seljak U., Kravtsov A. V., Wechsler R. H., 2005, MNRAS, 362, 1451
Mandelbaum R. et al., 2018, MNRAS, 481, 3170
Marra V., Quartin M., Amendola L., 2013, Phys. Rev. D, 88, 063004
McCarthy I. G., Schaye J., Bird S., Le Brun A. M. C., 2017, MNRAS, 465, 2936
Mead A. J., Heymans C., Lombriser L., Peacock J. A., Steele O. I., Winther H. A., 2016, MNRAS, 459, 1468
Mead A. J., Tröster T., Heymans C., Van Waerbeke L., McCarthy I. G., 2020, A&A, 641, A130
Mead A. J., Brieden S., Tröster T., Heymans C., 2021, MNRAS, 502, 1401
Mohammed I., Gnedin N. Y., 2018, ApJ, 863, 173
Möller A., de Boissière T., 2020, MNRAS, 491, 4277
Möller A. et al., 2022, MNRAS, 514, 5159
Myles J. et al., 2021, MNRAS, 505, 4249
Navarro J. F., Frenk C. S., White S. D. M., 1997, ApJ, 490, 493
Pan Z. et al., 2023, Phys. Rev. D, 108, 122005
Paopiamsap A., Porqueres N., Alonso D., Harnois-Deraps J., Leonard C. D., 2024, The Open Journal of Astrophysics, 7, 34
Planck Collaboration VI, 2020a, A&A, 641, A6
Planck Collaboration VIII, 2020b, A&A, 641, A8
Preston C., Amon A., Efstathiou G., 2023, MNRAS, 525, 5554
Prince H., Dunkley J., 2019, Phys. Rev. D, 100, 083502
Qu H., Sako M., Möller A., Doux C., 2021, AJ, 162, 67
Qu H. et al., 2024, ApJ, 964, 134
Quartin M., Marra V., Amendola L., 2014, Phys. Rev. D, 89, 023009
Rubin D. et al., 2023, preprint (arXiv:2311.12098)
Sánchez B. O. et al., 2024, ApJ, 975, 5
Schneider A., Teyssier R., 2015, J. Cosmol. Astropart. Phys., 2015, 049
Schneider A., Teyssier R., Stadel J., Chisari N. E., Le Brun A. M. C., Amara A., Refregier A., 2019, J. Cosmol. Astropart. Phys., 2019, 020
Shah P. et al., 2024a, MNRAS, 536, 946
Shah P. et al., 2024b, MNRAS, 532, 932
Sheth R. K., Mo H. J., Tormen G., 2001, MNRAS, 323, 1
Smith R. E. et al., 2003, MNRAS, 341, 1311
Sullivan M. et al., 2006, ApJ, 648, 868
Takahashi R., Sato M., Nishimichi T., Taruya A., Oguri M., 2012, ApJ, 761, 152
Terasawa R. et al., 2024, preprint (arXiv:2403.20323)
van Daalen M. P., McCarthy I. G., Schaye J., 2020, MNRAS, 491, 2424
Vincenzi M. et al., 2024, ApJ, 975, 86
Virtanen P. et al., 2020, Nat. Methods, 17, 261
Wang J., Bose S., Frenk C. S., Gao L., Jenkins A., Springel V., White S. D. M., 2020, Nature, 585, 39
Zhao D. H., Jing Y. P., Mo H. J., Börner G., 2009, ApJ, 707, 354
Zheng H., Bose S., Frenk C. S., Gao L., Jenkins A., Liao S., Liu Y., Wang J., 2024, MNRAS, 528, 7300
Zumalacárregui M., Seljak U., 2018, Phys. Rev. Lett., 121, 141101

APPENDIX A: SYSTEMATIC ERROR ESTIMATION

A1 The lensing likelihood

Although we have given plausible reasons for our assignment of the likelihood, doubts may still arise on its validity. One may worry about the ability of the sin/arcsin distribution to accurately represent the non-Gaussianity of intrinsic effects and residual contamination by non-SN Ia. Also, bias corrections adjust the mean of the residual distribution in bins to account for selection effects.

The Bayesian framework of estimated credible intervals allows us to exploit rigorous theorems to establish whether a posterior or specified credible interval is accurate. We note that while the homogeneous Gaussian SN Ia likelihood $\mathcal{L}_G$ has been extensively tested against simulations (see for example Camilleri et al. 2024), even this commonly used likelihood remains (in the sense we explain below) unproven.

Constraints on parameters are normally quoted as credible intervals, defined to be the range in which the integrated probability mass takes the specified value. A credible interval is located arbitrarily: common choices are to centre it on the mean, the median, or define it as the region of highest probability density (such that the size of the interval in parameter space is minimized). An inference pipeline such as the one we have described in this paper is a process to assign an *estimated* posterior distribution $\hat{p}(\theta|d)$ to model parameters θ given the data d. Intuitively, one may anticipate that if the estimated posterior correctly reproduces *all* of the credible intervals (with arbitrary location) of the true distribution p, then the posterior estimation is correct and $\hat{p} = p$. This was made rigorous in Lemos et al. (2023), who also give efficient methods for the computation.

Their method can be summarized as follows:

(i) choose a credibile level $1 - \alpha$, a proposal function g for the centre of the credibile interval θ_r, and a distance metric on the space of model parameters $s(\theta_1, \theta_2)$;

(ii) generate $i = 1 \dots N_{\rm sim}$ simulations of data vectors d_i drawing truth model parameters θ_i^* from the prior;

(iii) for each simulation i, construct the estimated posterior $\hat{p}_i$ and draw $j = 1 \dots N_{\rm sample}$ samples θ_{ij} from it;

(iv) the coverage probability for each simulation is $f_i = (1/N_{\rm sample}) \sum_j \mathcal{I}[s(\theta_{ij}, \theta_r) < s(\theta_{i,*}, \theta_r)]$ where $\mathcal{I}$ is the indicator function; and

(v) the expected coverage probability (ECP) for the estimated posterior method is then $\mathrm{ECP} = (1/N_{\mathrm{sim}}) \sum_i \mathcal{I}(f_i < 1 - \alpha)$.

If the ECP $= 1 - \alpha$ for all α and proposal functions g, then theorem 3 of Lemos et al. (2023) states that $\hat{p} = p$. In our context, this procedure represents a comparison of our analytic likelihood to an implicitly defined simulation-based likelihood that is deemed to be the truth.

We adopt three choices for g. We validate the regions of highest probability density (HPD) of the 1D marginalized distribution of A_{mod}, a uniform $g = \mathcal{U}(0.2, 2.5)$, and a normal $g = \mathcal{N}(0.75, 0.5)$ (i.e. in the vicinity of the median). The distance metric is $s(\theta_1, \theta_2) = |\theta_1 - \theta_2|$. We generate 240 simulations using the SNANA software (Kessler et al. 2009) with pipeline coordinator PIPPIN (Hinton & Brout 2020), 10 for each uniformly spaced A_{mod} value between the limits of the prior $A_{\mathrm{mod}} \in (0.2, 2.5)$. The simulations mimic the observing conditions and selection functions of the DES SN Ia survey, and are processed using the same pipeline as used for the real data, including adjustments for bias corrections. For each simulation, we sample 10^4 times from the posterior.

Fig. A1 shows the results. Although the HPD credible intervals (our preferred statistic) are all underconfident, the likelihood shows evidence of inaccuracy at the ~ 10 per cent level, and credible intervals in the vicinity of the median are somewhat overconfident. We can approximately convert this inaccuracy in the credible interval to a systematic error in A_{mod} in the following way: for a given location and desired credible interval $1 - \alpha$, interpolate the ECP until it matches $1 - \alpha$, and then re-evaluate the statistic at the credible interval matching this ECP. For example for the 68 per cent HDR constraint, we see the ECP (the y-axis on the upper panel of Fig. A1) that matches this corresponds to a ~ 59 per cent credible interval (the x-axis) for our estimated posterior. Re-evaluating the posterior with this revised interval leads to a constraint of $A_{\mathrm{mod}} < 0.90$, indicating our result was conservative by $\Delta A_{\mathrm{mod}} \sim 0.19$. Evaluations of other intervals at such intermediate levels of credibility lead to similar, or smaller, systematic error estimates.

We therefore assign $\Delta A_{\mathrm{mod}} = 0.19$ as the systematic error due to our likelihood assignment.

A2 Cosmological priors

It has been noted in the literature that assigning CMB priors to the amplitude of linear fluctuations can result in galaxy shear analyses preferring greater power spectrum suppression compared to adopting a wider prior (see fig. 6 of García-García et al. 2024 and fig. 11 of Terasawa et al. 2024). This is likely due the combined influence of linear and intermediate scales on galaxy shear data, which we do not expect to occur for SN Ia lensing constraints (see Fig. 2). To check this, we have repeated our analysis using priors derived from combining the DES 3×2pt (Abbott et al. 2022) and BAOs derived from the Sloan Digital Sky Survey (SDSS) (as summarized in Alam et al. 2021) (but retaining the *Planck* constraint on n_s). Note, *we do not alter the reference benchmark where* $A_{\mathrm{mod}} = 1$ *refers to fluctuations on all scales being consistent with the CMB in dark matter only* ΛCDM. This would represent a change of our baseline unit rather than any physical effect, and inhibit comparison of the values derived here to each other or the literature.

The change of prior affects our A_{mod} mean value at the level of $\Delta A_{\mathrm{mod}} \sim 0.01$. This is confirmed by Fig. 3, as the posteriors for large and small-scale fluctuation amplitudes are largely independent. Additionally varying n_s within the constraints allowed by the CMB results in a similar very small variation. We do not consider variations

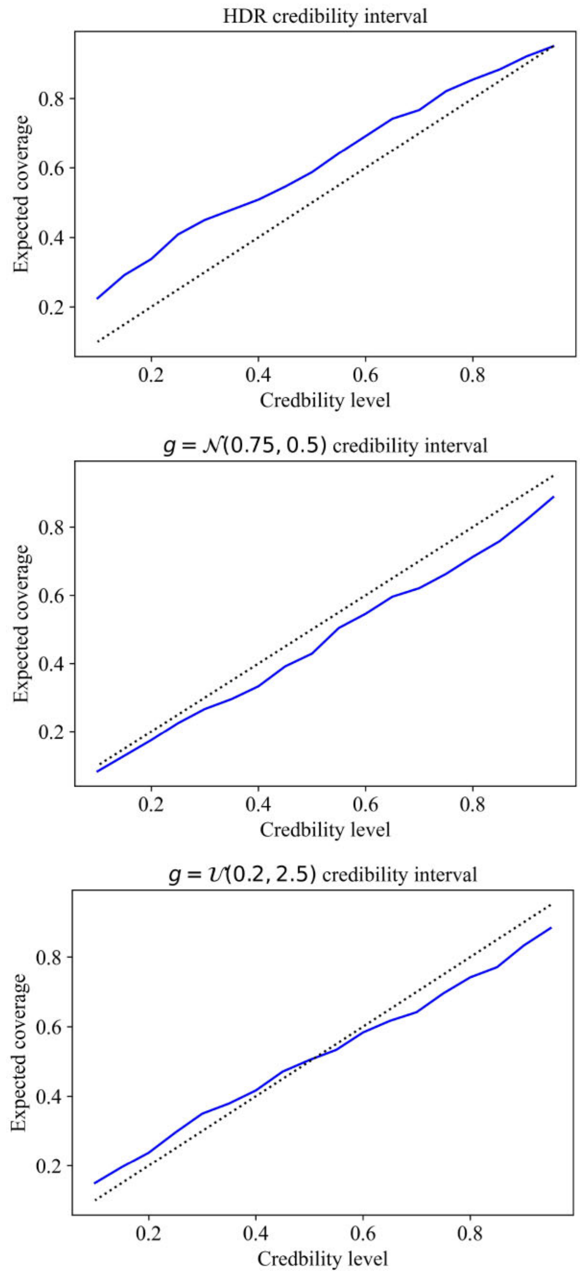

Figure A1. Graphs of the expected coverage probability (ECP) (solid line) against the specified credible interval for three choices of the credible interval location proposal function g. The x-axis is the integrated probability mass within the credible interval, and the y-axis are the results of the validation procedure outlined in the text above. The correct case is the dashed line. An underconfident likelihood would result in the solid line above the dashed line: the truthful credible interval level $1 - \alpha$ is larger than the desired input. Conversely, an overconfident likelihood would lie under. A biased likelihood would mix underconfidence in some intervals with overconfidence elsewhere. *Upper panel.* The estimation of the highest-density credible interval is underconfident by between 0 per cent and 20 per cent. *Middle panel.* The intervals concentrated around the median are overconfident by up to ~ 7 per cent. *Lower panel.* The intervals randomly located across the prior show the likelihood is biased to a similar degree, confirming the results of the upper two panels.

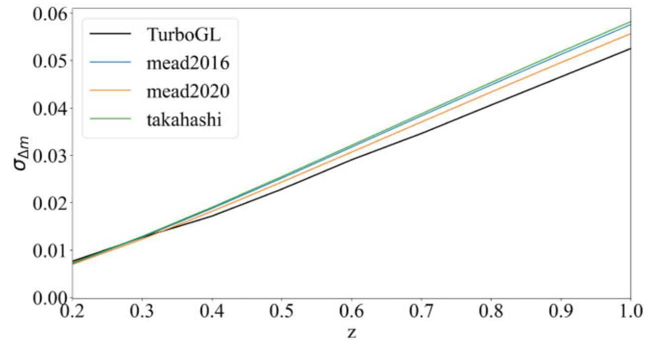

Figure A2. The standard deviation of the lensing pdf (in magnitudes) by redshift. The literature models are as described in Mead et al. (2016, 2020) and Takahashi et al. (2012), respectively (coloured lines), and the calculation of $\sigma_{\Delta m}$ is made with equation (5) with $k_{\max} = 10^3$. We compare this to the pdf we calculate using TURBOGL (black line).

in the sum of neutrino masses as this is one of the physical effects expected to be captured in the parameter $A_{\rm mod}$.

A3 Variation between TURBOGL and power spectrum emulators

We have used TURBOGL to construct our lensing pdf, and this forms our benchmark with respect to our $A_{\rm mod,S}$ result is obtained. Nevertheless, for the purposes of comparing with literature results, it is worthwhile to examine differences in lensing predictions from TURBOGL to power spectrum emulators like HMCODE2020.

Following the arguments of Marra et al. (2013), we examine the second moment of the lensing pdf. This directly relates to the $A_{\rm mod}$ parameter, and the shape of the lensing pdf is broadly universal, so the higher moments that drive our constraints scale in proportion to the standard deviation. We assign error budgets to the following potential inaccuracies: (1) the use of linearization in weak lensing, (2) the halo mass function calibration of Sheth et al. (2001), (3) the halo concentration relation of Zhao et al. (2009), and (4) uncertainties in the emulation of the power spectrum.

The first three were determined in Marra et al. (2013) as 5 per cent, 3 per cent, and 3 per cent, respectively and we adopt these estimates. For the last, we plot the variation in $\sigma_{\Delta m}$ (as determined from equation 5 for $k_{\max} = 10^3$) for the power spectrum models of Takahashi et al. (2012) and Mead et al. (2016, 2020) alongside our results derived from TURBOGL in Fig. A2. We adopt the median variation of 6 per cent as our systematic error for this component. Adding these errors in quadrature gives a total of 9 per cent.

A4 Summary

To recap, we estimate systematic errors of 0.19 for the likelihood, 0.01 for cosmological priors, and 0.09 for our lensing pdf. These add in quadrature to a total systematic error of $\Delta A_{\rm mod} = 0.21$.

[1]*Department of Physics & Astronomy, University College London, Gower Street, London WC1E 6BT, UK*
[2]*School of Mathematics and Physics, University of Queensland, Brisbane, QLD 4072, Australia*
[3]*Department of Physics, University of Oxford, Denys Wilkinson Building, Keble Road, Oxford OX1 3RH, UK*
[4]*The Research School of Astronomy and Astrophysics, Australian National University, ACT 2601, Australia*
[5]*Center for Astrophysics | Harvard & Smithsonian, 60 Garden Street, Cambridge, MA 02138, USA*
[6]*Institut d'Estudis Espacials de Catalunya (IEEC), E-08034 Barcelona, Spain*
[7]*Institute of Space Sciences (ICE, CSIC), Campus UAB, Carrer de Can Magrans, s/n, E-08193 Barcelona, Spain*
[8]*SLAC National Accelerator Laboratory, Menlo Park, CA 94025, USA*
[9]*Department of Physics, University of Michigan, Ann Arbor, MI 48109, USA*
[10]*Department of Physics and Astronomy, University of Pennsylvania, Philadelphia, PA 19104, USA*
[11]*Centre for Gravitational Astrophysics, College of Science, The Australian National University, ACT 2601, Australia*
[12]*Centre for Astrophysics & Supercomputing, Swinburne University of Technology, Victoria 3122, Australia*
[13]*School of Physics and Astronomy, University of Southampton, Southampton SO17 1BJ, UK*
[14]*Fermi National Accelerator Laboratory, P. O. Box 500, Batavia, IL 60510, USA*
[15]*Laboratório Interinstitucional de e-Astronomia – LIneA, Rua Gal. José Cristino 77, Rio de Janeiro, RJ-20921-400, Brazil*
[16]*Department of Physics, Northeastern University, Boston, MA 02115, USA*
[17]*Instituto de Astrofisica de Canarias, E-38205 La Laguna, Tenerife, Spain*
[18]*Dpto. Astrofísica, Universidad de La Laguna, E-38206 La Laguna, Tenerife, Spain*
[19]*Institut de Física d'Altes Energies (IFAE), The Barcelona Institute of Science and Technology, Campus UAB, E-08193 Bellaterra (Barcelona) Spain*
[20]*Jodrell Bank Center for Astrophysics, School of Physics and Astronomy, University of Manchester, Oxford Road, Manchester M13 9PL, UK*
[21]*University of Nottingham, School of Physics and Astronomy, Nottingham NG7 2RD, UK*
[22]*Hamburger Sternwarte, Universität Hamburg, Gojenbergsweg 112, D-21029 Hamburg, Germany*
[23]*Department of Physics, IIT Hyderabad, Kandi, Telangana 502285, India*
[24]*Jet Propulsion Laboratory, California Institute of Technology, 1200 East California Blvd, MC 249-17, Pasadena, CA 91125, USA*
[25]*Institute of Theoretical Astrophysics, University of Oslo, P.O. Box 1029 Blindern, NO-0315 Oslo, Norway*
[26]*Kavli Institute for Cosmological Physics, University of Chicago, Chicago, IL 60637, USA*
[27]*Instituto de Fisica Teorica UAM/CSIC, Universidad Autonoma de Madrid, E-28049 Madrid, Spain*
[28]*Institute of Cosmology and Gravitation, University of Portsmouth, Portsmouth PO1 3FX, UK*
[29]*University Observatory, Faculty of Physics, Ludwig-Maximilians-Universität, Scheinerstr. 1, D-81679 Munich, Germany*
[30]*Center for Astrophysical Surveys, National Center for Supercomputing Applications, 1205 West Clark St, Urbana, IL 61801, USA*
[31]*Department of Astronomy, University of Illinois at Urbana-Champaign, 1002 W. Green Street, Urbana, IL 61801, USA*
[32]*Santa Cruz Institute for Particle Physics, Santa Cruz, CA 95064, USA*
[33]*Center for Cosmology and Astro-Particle Physics, The Ohio State University, Columbus, OH 43210, USA*
[34]*Department of Physics, The Ohio State University, Columbus, OH 43210, USA*
[35]*Jet Propulsion Laboratory, California Institute of Technology, 4800 Oak Grove Dr, Pasadena, CA 91109, USA*
[36]*George P. and Cynthia Woods Mitchell Institute for Fundamental Physics and Astronomy, Department of Physics and Astronomy, Texas A&M University, College Station, TX 77843, USA*
[37]*Laboratoire de Physique Subatomique et de Cosmologie, Avenue des Martyrs F-38026, Grenoble, France*
[38]*Institució Catalana de Recerca i Estudis Avançats, E-08010 Barcelona, Spain*
[39]*Department of Physics, Carnegie Mellon University, Pittsburgh, Pennsylvania 15312, USA*
[40]*Observatório Nacional, Rua Gal. José Cristino 77, Rio de Janeiro, RJ-20921-400, Brazil*
[41]*Kavli Institute for Particle Astrophysics & Cosmology, P. O. Box 2450, Stanford University, Stanford, CA 94305, USA*

[42] *Centro de Investigaciones Energéticas, Medioambientales y Tecnológicas (CIEMAT), Madrid, Spain*
[43] *Ruhr University Bochum, Faculty of Physics and Astronomy, Astronomical Institute, German Centre for Cosmological Lensing, D-44780 Bochum, Germany*
[44] *Physics Department, Lancaster University, Lancaster LA1 4YB, UK*
[45] *Computer Science and Mathematics Division, Oak Ridge National Laboratory, Oak Ridge, TN 37831, USA*
[46] *Department of Astronomy, University of California, Berkeley, 501 Campbell Hall, Berkeley, CA 94720, USA*
[47] *Lawrence Berkeley National Laboratory, 1 Cyclotron Road, Berkeley, CA 94720, USA*

This paper has been typeset from a TEX/LATEX file prepared by the author.